HHS Public Access

Author manuscript

J Mater Res. Author manuscript; available in PMC 2019 January 27.

Published in final edited form as:

J Mater Res. 2018 July 27; 33(14): 1948–1959. doi:10.1557/jmr.2018.112.

Systematic characterization of 3D-printed PCL/β-TCP scaffolds for biomedical devices and bone tissue engineering: influence of composition and porosity

Arnaud Bruyas[§],
Department of Orthopaedic Surgery, Stanford University, 300 Pasteur Drive, 94305, Stanford CA

Frank Lou[§],
Department of Mechanical Engineering, Stanford University, 440 Escondido Mall, 94305, Stanford CA

Alexander M. Stahl,
Department of Chemistry, Orthopaedic Surgery, Stanford University, 300 Pasteur Drive, 94305, Stanford CA

Michael Gardner,
Department of Orthopaedic Surgery, Stanford University, 300 Pasteur Drive, 94305, Stanford CA

William Maloney,
Department of Orthopaedic Surgery, Stanford University, 300 Pasteur Drive, 94305, Stanford CA

Stuart Goodman, and
Department of Orthopaedic Surgery, Stanford University, 300 Pasteur Drive, 94305, Stanford CA

Yunzhi Peter Yang
Department of Orthopaedic Surgery, Bioengineering, Material Science and Engineering, Stanford University, 300 Pasteur Drive, 94305, Stanford CA

Abstract

This work aims at providing guidance through systematic experimental characterization, for the design of 3D printed scaffolds for potential orthopaedic applications, focusing on fused deposition modeling (FDM) with a composite of clinically available polycaprolactone (PCL) and β-tricalcium phosphate (β-TCP). First, we studied the effect of the chemical composition (0% to 60% β-TCP/PCL) on the scaffold's properties. We showed that surface roughness and contact angle were respectively proportional and inversely proportional to the amount of β-TCP, and that degradation rate increased with the amount of ceramic. Biologically, the addition of β-TCP enhanced proliferation and osteogenic differentiation of C3H10. Secondly, we systematically investigated the effect of the composition and the porosity on the 3D printed scaffold mechanical properties. Both an increasing amount of β-TCP and a decreasing porosity augmented the apparent Young's modulus of the 3D printed scaffolds. Third, as a proof-of-concept, a novel multi-material biomimetic implant was designed and fabricated for potential disk replacement.

Correspondence to: Yunzhi Peter Yang.

[§]Both authors contributed equally to this work.

Keywords

composite; bone; biomimetic

Introduction

Design and manufacturing of synthetic scaffolds to stimulate bone repair has been extensively studied. [1][2][3][4] It is reported that a construct should ideally present the following properties: biocompatibility, high porosity with interconnected pores to allow cell ingrowth, sufficient mechanical strength, promotion of cell adhesion (osteoconductive) and activity (osteoinductive), appropriate degradation, and custom-fit geometry. [3] The design of a construct is therefore complex, and different manufacturing processes have been explored in this regard, such as casting, molding, or electrospinning. Recently, additive manufacturing (AM) has received increasing attention in medical devices and tissue engineering, because it allows the manufacturing of constructs with a controllable and accurate material layout, leading to a high potential for complex geometries and better control over the porosity and pore layout in the construct. [5] [6] [7] In particular, Fused Deposition Modeling (FDM) is of interest for bone tissue engineering, because of its ease of use, the variety of biocompatible polymers and composites that can be exploited, and because porous structures can be accurately generated. Numerous studies have been published regarding this topic, and a large number of geometries as well as materials have been explored. [8][9][10][11]

Regarding material composition, medical grade poly(ε-caprolactone) (PCL) and beta tricalcium phosphate (β-TCP) are two widely used materials for orthopaedic applications. [1][5][12] PCL is a biocompatible synthetic polymer that is employed for biodegradable implants, due to its biocompatibility, long-term biodegradability, FDA approval and relatively low cost. [8][13] In addition, PCL can easily be manufactured and manipulated, thanks to its low melting point, its ease of mixture with other materials (polymers and ceramics), and its compatibility with most AM methods, in particular FDM. [14] β-TCP is a calcium phosphate derivative, similar to the calcium phosphate material that comprises between 60-70% of natural bone, thus presenting an inherent biomimetic potential. It is biodegradable and has been demonstrated to have osteoconductive properties in encouraging new bone growth, thus reducing patient recovery time due to the generation of natural bone tissue. [15] The combination of these two materials offers unique properties and presents great interest for regenerative medicine, and many studies have been conducted on this particular composite for medical devices, implants and constructs for orthopaedic applications. [16] [17] [18] During the design of the construct, its porosity and its composition must be carefully defined, since both parameters can be related to the scaffold's properties (chemical, physical and biological) known to be of influence in tissue engineering, such as surface composition, degradation, stiffness, surface morphology and hydrophilicity, cell proliferation and differentiation. Several studies have linked some of these properties to the porosity and/or the composition of the construct. For instance, Huang et al. [14] showed that the addition of β-TCP in PCL improved the 3D printed scaffold's mechanical performance, and Yeo et al. studied in detail the degradation of PCL/ β-TCP

scaffolds (80:20) both in vitro and in vivo. [16] Hollister et al. [19][20] focused on the relationship between porosity and mechanical stiffness to mimic different types of bone tissue, and Shin et al. [21] highlighted the influence of calcium phosphate on osteogenic differentiation of human mesenchymal stem cells, demonstrating an increasing ALP activity of scaffolds with calcium phosphate compare to PCL only. However, the definition of both the composition and the porosity for a given application often remains the result of a trial and error approach, which seems largely sub-optimal given the number of properties and their inter-dependability.

In this paper, we report on a systematic approach to this problem, by manufacturing and assessing the properties of 3D printed PCL/ β-TCP scaffolds with different compositions and porosities. We first focused on the effect of the composition. For that purpose, we synthesized PCL/β-TCP composites with different proportions of ceramic (0%, 20%, 40%, 60% β-TCP) and 3D printed non-porous scaffolds. For each composition, we examined the surface morphology, evaluated the hydrophilicity, quantified the degradation speed and determined the mechanical properties of the material. We then performed in-vitro biological experiments in order to assess the composition effect on cell proliferation and osteogenic differentiation. Next, we systematically assessed the effect of both the composition and the porosity on mechanical properties. We produced 20 groups of scaffolds with different porosities and composition, measured their volume and characterized their mechanical performances. In the last part of the paper, as a proof of concept, a 3D printed implant composed of multiple materials and porosities was designed and fabricated for the application of disc replacement. The choice of the design parameters was detailed and a prototype was manufactured.

Experimental

A/ Synthesis and composition analysis of PCL/ β-TCP materials

Polycaprolactone (Sigma-Aldrich, USA) and β-TCP powder with particle size averaging 100nm (Berkeley Advanced Materials Inc., USA) were weighed with respect to the required PCL/ β-TCP ratio. 10% (wt/v) PCL solution and 5% (wt/v) β-TCP solution in dimethylformamide were prepared at 80°C and stirred for 3 hours, before being mixed together and thoroughly stirred for another 1 hour. This solution was then precipitated in a large volume of water at room temperature to remove the solvent. The material was then dried for 24h at room temperature, and manually cut into pellets of approximately 5mm in diameter. This synthesis process was repeated for each ratio of PCL to β-TCP explored in this study: 100/0, 80/20, 60/40 and 40/60.

Similar to the test performed by Lepoittevin, et.al, [22] the composition of the synthesized composites was validated by thermal gravimetric analysis (TGA), using a TA instrument Q500 TGA (TA instrument, USA). Briefly, the samples were heated up to 550°C with a constant increase of 20°C per minute, while monitoring their mass over time. Because of the thermal properties of both materials, the remaining mass at the end of the test was considered to be pure β-TCP.

B/ Filament fabrication and scaffold 3D printing

Using an in-house built screw extruder (see Figure S1), the solid pellets of PCL/ β-TCP were melted at 90°C and extruded into a filament of constant diameter for FDM 3D printing. Average filament diameter for each group was measured and the values were used for each group respectively during the 3D printing process. Scaffolds were manufactured using a Lulzbot Mini (Aleph Objects Inc, USA) with a nozzle of 500μm. The printing temperature was set to 160°C so that each ratio could be printed smoothly. The layer thickness was set to 200μm, each layer being constituted of parallel struts with an orientation of 90° relative to the previous layer. The printing speed was set to 5mm/s, and was calibrated to deposit struts of width ranging from 350μm to 400μm. Two types of scaffold were manufactured. For surface characterization, and biological studies, disks of diameter 10mm, thickness 600μm and strut distance 0.4mm (0% porosity) were manufactured, resulting in a scaffold with a plain surface. For mechanical testing, the specimens were cylinders of diameter 10mm and height 5mm. 5 different porosities were explored for each material composition. They correspond to 5 different strut distances: 0.4mm, 0.5mm, 0.71mm, 1.25mm and 2.5mm. 0.4mm is the theoretical distance for a porosity of 0%, and 2.5mm has been empirically defined as the maximum value that still ensures scaffold integrity.

C/ Surface characterization

Hydrophobicity was evaluated using a contact angle goniometer, Ramé-Hart 290 (Ramé-Hart instrument co., USA). Briefly, a droplet (4μL) was deposited at the center of the disc scaffold, and the contact angle was measured 1 minute after deposition using image processing. Five samples were tested for each group. Because the contact angle is linked to surface chemistry as well as morphology, and because 3D printing affects surface morphology, two assays were carried out. The first assay aimed at studying the impact of the composition only. To homogenize the surfaces after 3D printing, post-processing was performed. The scaffolds were placed in an oven at 80°C onto a glass substrate for 10 minutes in order to melt the samples and obtain similar surfaces for all the compositions. The second assay was performed on the scaffolds directly after printing in order to observe the influence of both the material composition and the manufacturing process.

The morphology of the surface was evaluated qualitatively using second electron emission imaging. The samples were first cleaned in ethanol and cut to size using a scalpel. Samples were sputter-coated with gold (10 nm) (SPI Sputter, SPI Supplier Division of Structure Prob Inc., West Chester, PA, USA). A scanning electron microscope (SEM, Zeiss Sigma FESEM) was then used to image the samples at three different magnifications: 150, 1000, and 10000, with an acceleration voltage of 3 kV.

Surface roughness (arithmetic average roughness Ra) of the disk scaffolds was quantified using a profilometer (Dektak XT, Bruker, MA, USA). The profiles were measured over a line of 1mm length following a single strut, with a stylus force of 1mg and a measuring range of 6.5μm. 5 samples were tested per group.

D/ Degradation

Because PCL is a slow biodegradable polymer, accelerated degradation was performed following the protocol described by Lam et al. [23] Pieces of filaments (length 20mm) were used as specimens to quantify the degradation of the material itself and not the scaffold after printing. The specimens were immerged in a 5M NaOH solution (15mL) and incubated at 37°C. At predefined timepoints, they were removed, dried in an oven at 30°C for 45 minutes to remove any liquid, and weighed. Degradation was then quantified through measuring mass loss, i.e, the change in mass of the bulk recovered filament sample throughout the duration of the experiment.

E/ Biological study

For all biological studies, multi-potent mouse C3H10T1/2 fibroblasts (ATCC, USA) were used as a model to study osteogenic differentiation of mesenchymal stem cells. They were cultured in DMEM (Life Technologies, USA) supplemented with 10% fetal bovine serum (FBS, Life Technologies, USA) and 1% PS. Medium was changed every two day. Cells were incubated at 37°C, 5% CO_2 in a humidified incubator.

Biological experiments were performed using flat non-porous scaffolds in order to assess the impact of the composition only and for practical reason of image analysis of non-transparent samples (details are provided in supplementary material 2). After manufacturing, disc samples were immersed in a 70% ethanol solution for 20 min, rinsed in PBS 3 times and dried overnight. Cell seeding was performed in 24 wells culture plates by depositing cells suspended in media on the surface of the disc with a concentration of 0.8×10^4 cells/cm^2, incubating them for 20 min before filling the well with 1mL of media. Cell proliferation and osteogenic differentiation were both assessed at day 1, 7, 11. Proliferation was evaluated by moving the scaffolds to new wells, detaching the cells from the scaffold using 0.05% trypsin (Life Technologies, USA), suspending them in media, and counting them using a Z2 particle counter (Beckman Coulter, USA). For cell differentiation, Alkaline Phosphatase (ALP) activity of cells was assessed through semi-quantitative staining. Alkaline Phosphatase kit (Sigma-Aldrich, USA) was used and the staining was performed following the manufacturer instructions. At designated time-points, cells were fixed for 1 minute in 3.7% formaldehyde and samples were incubated for 1 hour with ALP stain. After staining, the scaffolds were imaged and the ALP levels were quantified using image processing performed with Matlab R2013 (MathWorks, USA). Briefly, color features of the images of the scaffolds were extracted, quantified, and the pixel values were averaged over the entire surface of the scaffold. For each composition, the obtained values at day 7 and 11 were normalized using the average value at day 1.

F/ Porosity measurement

To assess the actual porosity of each scaffold, they were imaged using a micro-CT imaging device eXplore CT120 (TriFoil Imaging, USA). Reconstruction was performed using MicroView software (Parallax Innovations, Canada). Each composition was processed independently because of their different sensitivities to X-ray imaging. For each, a threshold value was identified using the automatic tool provided by the software. Using this value, the

volume of each individual sample was computed. To get the porosity p, the construct volume Vc was compared to the overall volume of the cylinder Vt, using equation 1.

$$p = 1-(Vc/Vt)$$

G/ Mechanical analysis

First, the mechanical properties of the bulk materials were evaluated in order to examine the properties of the material independently of the manufacturing process. For this purpose, 5 cm pieces of filament were directly used as specimens. Tensile testing was performed using an Instron 5944 uniaxial testing system with a 2 kN load-cell (Instron Corporation, Norwood, MA). A preload of 1N was applied, at a speed of 1% strain/s until 25% strain. The values of the Young's modulus as well as the tensile strength at zero slope were extracted, the first one being the value of the initial slope of the stress-strain curve, the second being the ordinate of the zero slope point of the curve. Five specimens were tested per material composition.

Then, 3D printed porous scaffolds were mechanically tested in compression using the same instrument, following guidelines adapted from Huang, et al. [14] A preload of 1N was applied, and tests were performed at a speed of 1% strain/s until 25% strain. Five porosities were independently tested for each composition in order to study the influence of both the amount of β-TCP and the porosity on the mechanical properties. Five specimens were tested for each group, and for each specimen, the apparent Young's modulus and the yield strength at 1% were measured. The first one was identified as the slope of the initial linear portion of the stress-strain curve. The second one corresponds to the ordinate of the intersection between the stress-strain curve and a line with a slope equal to the Young's modulus starting at an offset of 1% strain.

H/ Manufacturing of a multi-material 3D printed implant

In order to 3D print a single piece construct consisting of several materials, an algorithm was developed. Knowing the layout of the construct and the position of each material in the construct's bulk volume, the corresponding length of filament for each volume required was computed. The filament pieces were then manually fused in the order in which the printing would complete each separate section to form a single multi-material construct. The recomposed filament was then used by the printer to manufacture the multi-material construct in a single iteration, with each major section of the construct utilizing a different material. To prove the feasibility of multi-material constructs, a novel implant for disc reconstruction was proposed. The design as well as a prototype are detailed in the Results and Discussion sections.

I/ Statistical analysis

Data are presented using mean ± standard deviation. Statistical analyses were performed using t-test method when two groups were involved, and one-way analysis of variance (ANOVA) with ad-hoc Tukey's test for three or more groups. Differences were considered

significant for $p < 0.05$, as labeled in figures by the * symbol. Analyses were performed using Matlab R2013 software (MathWorks, USA).

Results and discussion

A/ Material composition

Using the TGA curves presented in Figure 1 (a), the ratios of β-TCP in the samples were quantified as the remaining mass at 550°C. The values are 2.62%, 21.06%, 41.55%, 59.31% for theoretical compositions of 0%, 20%, 40%, and 60% β-TCP, respectively, which represents relative errors of 2.62%, 1.06%, 1.55% and 0.69%, respectively. This disparity can either be the result of impurities in PCL and/or experimental errors. This analysis validates the material composition after synthesis, and therefore confirms that the solvent method used in this study efficiently mixes PCL and β-TCP with a ratio up to 60% ceramic. For future reference, higher amounts of β-TCP were attempted, but the synthesis failed as the amount of PCL was too low to bind such a large amount of ceramic, resulting in a collapsing composite after precipitation. Figure 1 (b) presents the differential thermogravimetric curves, which are the first derivative of the TGA curves, providing further information on material thermal degradation. The abscissa of the larger peak for each composition are 378.3°C, 398.3°C, 402.1°C and 409.2°C, respectively for 0%, 20%, 40% and 60% of β-TCP, showing a slight increase in thermal stability due to the addition of β-TCP, which corroborates the results presented by Huang, et. al. [14]

Filament diameters following extrusion were also measured, averaging 2.75 mm ± 0.10, 2.43 mm ± 0.08, 2.45 mm ± 0.03, and 2.66 mm ± 0.04, respectively for β-TCP ratios of 0%, 20%, 40% and 60%.

B/ Composition influence

1/ Surface characterization—Contact angle tests were first performed on post-processed scaffolds in order to quantify the influence of the composition alone. As shown in Figure 2 (a), all values are under 90°C (between 70° and 80°), indicating that the materials tend to be hydrophilic. Moreover, a small decrease in contact angle is showed when the amount of ceramic is increasing, with statistical significance between 0%, 20% and 60%. Figure 2 (b) presents the results of similar tests on scaffolds without post-processing, in order to assess both the influence of the composition and the manufacturing process on the contact angle. Contrary to the previous test, no significant difference is noted between the different groups although their chemical compositions are different. Similar results are demonstrated in [25], where pure PCL presents a contact angle of 75°, while the addition of β-TCP did not significantly affect the contact angle. These two tests show that the surface morphology resulting from FDM 3D printing has a non-negligible impact on surface hydrophilicity. This morphology is the result of the layer formation strut by strut, and is inherent to FDM 3D printing technology.

Surface morphology was observed using SEM imaging, presented in Figure 2 (c)-(f). Cross-sectional images are also introduced in Figure S3. At every scale, imaging shows a relatively smooth surface for pure PCL, and an increase in surface roughness for higher β-TCP ratios.

At low magnification (x150), the morphology is the result of two phenomena. First, the junction between struts of a single layer can be observed, resulting in linear ridges on the surface, as indicated in Figure 2 (c)-(f) I). This is the result of the strut by strut deposition of FDM 3D printing processes. Although careful calibration can attenuate it, it is related to the inherent variability of the process and therefore cannot be entirely removed. Second, the addition of ceramic nanoscopic powder is introducing bumps at the surface. At this scale, they are the results of aggregates of ceramic particles that assemble together because of the high surface tension of nanoparticles and the separation of the hydrophilic ceramic particles from the PCL matrix. Although both components of the composite were put in solution separately and thorough mixing was carried out, interaction between particles was evidently stronger. At ×1000 magnification, these aggregates can be better observed (Figure 2 (c)-(f) II)). Because of the extrusion process, they are usually under a thin layer of polymer, sometimes even creating holes in the surface of the material. Consequently, the higher the amount of ceramic in the composite, the rougher the surface will be. At high magnification (×10000), the ceramic particles can be distinguished, their average size being 100 nm (Figure 2 (c)-(f) III)). Some of them are apparent, but judging by the texture of the surface, not all of them seem to be exposed, and similar to aggregates, some of them are covered with a thin layer of polymer.

Surface roughness measurements Ra are introduced in Figure 2 g), with values of 178.3 ± 67.6 nm, 645.7 ± 84.7 nm, 1193.6 ± 97.6 nm, and 1837.6 ± 317.6 nm, respectively for β-TCP ratios of 0%, 20%, 40%, and 60%. A significant increase of Ra is observed for increasing amount of ceramic, confirming the observations of the SEM images.

2/ Degradation—Significant differences in degradation rates under accelerated condition were observed between the different materials depending on the ratio of ceramic to polymer utilized (Figure 3). Quantifiable mass loss in the two materials with higher ceramic content (60% and 40%) commenced within 24 hours, with the 60% filament experiencing over 50% mass loss within 10 hours. Lower ceramic content filament (20%) showed <5% mass loss after the total 54 hours period of the trial, and all samples of pure PCL filament experienced <1% mass loss over the same duration.

These results are consistent with results presented in similar studies. Indeed, polyester degradation under alkaline conditions is a well-known accelerated degradation protocol. [16] [23] [24] It is thought that polyester degradation under these conditions mimics typical degradation under aqueous conditions where ester-ester linkages are hydrolytically severed, breaking apart the bulk material. The presence of additional -OH ions from alkaline solution catalyzes this process, speeding up a degradation process that can require 3-4 years *in vivo.* [23] Lei, et. al suggested that the addition of β-TCP speeds up the degradation because β-TCP particles are only physically mixed in the composite, and submersion in the alkaline media frees the β-TCP particles to convert into its more thermodynamically favorable form of apatite in solution. [18] The void left by dissolving β-TCP particles additionally increases the available surface area for the aforementioned hydrolytic attack on ester-ester linkages, while also opening up more regions of β-TCP to be freed. Visually, it was noted that solutions further along in the degradation process possessed a white powder-like substance that precipitated along the bottom of the vials used for degradation; these are theorized to be

the aforementioned released β-TCP particles. Higher ceramic content filaments thus experienced accelerated rates of degradation due to the presence of more β-TCP particles, allowing for greater amounts of the ceramic to be released and quickening the rate at which the filaments lost structural integrity. As such, it is worth noting that the extremely high degradation rates of the higher ceramic content (40% and 60%) is a result of disassembly of the composite, i.e loss of structural integrity, in combination with our assay method of mass measurement of the samples, but not the dissolution/disappearance of the ceramic particles themselves. However, this result does offer an approach via manipulation of the ceramic ratio to control degradation rates, and further enables the creation of a bioresorbable bone implant that can ideally be designed to match the natural variations found in bone healing rates. [26]

3/ Mechanical properties of bulk material—Tensile tests were performed on filament shape material of different composition in order to assess the bulk mechanical properties, i.e the properties of the material before being affected by the manufacturing process (Figure 4 (a)). Both Young's modulus and yield strength are introduced in Figure 4 (b) and 4 (c). Young's modulus average values were 264 MPa, 355MPa, 495MPa and 1140 MPa, respectively for 0%, 20%, 40% and 60% of β-TCP content and yield strength average values were 14.2 MPa, 12.4 MPa, 10.74 MPa and 10.29 MPa for the same β-TCP ratios. Young's modulus quantifies the material stiffness, and increases with the amount of ceramic in the composite, with statistical significance between all the groups. The increase seems to be linear up to 40%, and displays a larger increase between 40% and 60%. The yield strength decreased compared to the amount of ceramic in the composite. It represents the maximum stress that can be applied to the material without permanent deformation. As a result, elasticity of PCL/β-TCP composite reduces with higher quantity of ceramic.

Theoretical models have been developed to estimate the Young's modulus of particulate-filled systems. [27] For spherical particles added in a polymeric phase, the simplest model equation has been identified by Einstein. [27] Under certain hypotheses (low ratio of particles, perfect adhesion between the two phases of the composite, particles much more rigid than the matrix) a linear dependency can be highlighted between the Young's modulus of the composite and the Young's modulus of the polymer, according to the volume ratio of particles. For large filler concentration, a more complex model has been developed by Kerner, [27] which under the same hypotheses predicts considerably more stiffening action of the filler compared to Einstein's model for higher particle concentration. Both these models support the results presented in Figure 4 (b),(c).

4/ Cell proliferation and differentiation—Figure 5 shows the proliferation results of mouse fibroblasts (C3H10 T1/2) at day 1, 7 and 11. At day 1, no significant difference was noted between groups, highlighting the fact that scaffold composition had no influence on cell attachment. Over the three time-points, the number of cells increased for all groups. Starting at day 7, the number of cells on the sample containing β-TCP became significantly higher than the number of cells on pure PCL scaffolds (about 50% more on average at day 11). Although it may seem that the number of cells slightly increased with the ceramic ratio at day 11, no statistical difference was shown over the different β-TCP ratios. The

proliferation study indicated that addition of ceramic improves cell proliferation compared to pure PCL. One possible explanation is the variation in surface morphology reported previously, since it has been shown that cells proliferate better on rougher surfaces, as rougher surfaces provide larger surface area for cell growth. [11]

Figure 6 (b) represents the relative ALP activity of the different groups for days 1, 7, and 11, and examples of scaffolds at day 11 after staining are introduced in Figure 6 (a). For composition of 0% and 20% β-TCP, no significant increase was shown over time, while 40% and 60% ratios indicated a significant increase of activity at day 11 compared to day 1 and 7, with respective increases of 5% and 10%. Moreover, the ALP activity seems to increase with the amount of β-TCP in the scaffold, with significant differences between 0% and 40%,60%, and between 20% and 60% (see Figure 6 (b)). These results highlight the impact of the addition of β-TCP on C3H10 osteogenic differentiation, and corresponding results can be found in the literature. Shin et. al demonstrated a higher ALP activity for human mesenchymal stem cells cultured on PCL/β-TCP compared to PCL only, pointing out a potential impact of the exposed β-TCP particles at the surface of the scaffold. [21] Similar results were shown by Polini et.al, where the addition of β-TCP in PCL nanofibers improved stem cell differentiation. [25]

The biological studies highlight the osteoconductive property of β-TCP and are in accordance with other studies on the impact of calcium phosphate based materials (β-TCP or hydroxyapatite) for both proliferation and differentiation of stem cells. [15] [25] It is not clear, however, if this impact is the result of differences in chemical surface properties or of differences in physical properties of the surface (hydrophobicity, roughness, stiffness). Although we tried to isolate the influence of the composition only, it is inherently linked to the physical properties through the manufacturing process. Post-processing techniques could be considered in order to modify physical properties and decrease the physical properties variability for more accurate assessment in the future.

C/ Effect of composition and porosity on mechanical properties

Characterization of the influence of porosity and composition on the mechanical properties of 3D constructs was performed in a systematic manner. 20 different groups were manufactured using FDM (Figure 7 (a)) with n=5 for each group. The average values of porosity for each group are presented in Figure 7 (d). As expected, porosity was mostly guided by the distance between each strut in the scaffold, and very low variation is noted between the β-TCP ratios. After being tested under compression, apparent Young's modulus and yield strength were computed for each group, as presented in Figure 7 (b) and 7 (c). These values respectively ranged from 12 MPa (β-TCP ratio: 60%, strut distance: 2.5mm) to 188 MPa (β-TCP ratio: 60%, strut distance: 0.4 mm), and 0.7 MPa (β-TCP ratio: 60%, strut distance: 2.5mm) to 15.4 MPa (β-TCP ratio: 0%, strut distance: 0.4 mm). In comparison, Gibson [28] tested cancellous bone from varying regions of the body and demonstrated Young's modulus values that varied between an order of magnitude of 10^0 MPa and 10^2 MPa, a range is similar to the Young's modulus range demonstrated in Figure 7 (b). This study could therefore be used to design and tailor constructs specific to the type of bone

considered in the application, improving its biomimicry, and hypothetically enhancing bone regeneration rates.

To assess the extent of the influence of the composition versus the porosity, each mechanical parameter was graphically related to the porosity in Figures 7 (e) and 7 (f). For the apparent Young's modulus, a linear trend can be identified, the slope being steeper with the amount of β-TCP. As a result, the composition of the construct has very little influence on its apparent Young's modulus for high porosity. For lower porosity, an increasing amount of ceramic results in higher Young's modulus. Comparing the values of the lowest porosity (close to 0%) to the results of the tensile tests performed on the same materials in a bulk form, a large discrepancy can be noted, especially for higher amounts of ceramic, which highlights the important influence of the FDM process and the geometry of the construct. Regarding yield strength (Figure 7 (f)), the curve of each composition overlays, underscoring the fact that β-TCP amount has very little influence and that the yield strength of a 3D construct is guided by the layout of its layers. Indeed, during compression testing, yield is the result of a collapse of the construct when loaded, which makes the geometrical layout of the construct of higher impact compared to the composition.

Interestingly, a similar apparent Young's modulus value can be achieved by constructs with very distinct design parameters. For instance, scaffolds with 15% porosity/0% β-TCP, and 45% porosity/60% β-TCP will both have an apparent Young's modulus of about 100 MPa. This overlap results in more freedom regarding construct design, and allows for researchers to take other parameters into consideration other than solely the mechanical performances, since these two vastly different compositions can result in the same mechanical values. For this purpose, results presented in this section and the rest of the paper can act as guidelines and assist in the design process.

E/ Multi-material implant for disc reconstruction: Proof of concept

Using the results previously presented, and to prove the feasibility of manufacturing multi-material constructs 3D printed in a single piece, a novel design for disc reconstruction is presented. Disc implants aim at replacing a collapsing disc between two vertebrae. Typically, they are composed of four assembled parts: two inner elements sliding between each other to allow relative movement between the vertebrae, placed in between two metallic endplates connecting the implant to each vertebrae. [29] An alternative design is introduced in Figure 8 (a), using the data collected in this study. For high stiffness and better osteoconduction, the two endplates consist of 45% porous material with a high amount of β-TCP. They are connected through a section of highly porous (70-75%) pure PCL designed to mimic biological cartilage stiffness and elasticity. Being 3D printed in a single piece, no assembly is required and the construct can be patient specific. A prototype is pictured in Figure 8 (b), validating the feasibility of single piece 3D printed constructs integrating multiple porosity and multiple composites.

Conclusion

In this paper, we systematically studied the influence of the composition and porosity of FDM 3D printed PCL/β-TCP constructs on properties that are of interest for bone tissue

engineering applications, namely surface morphology and hydrophilicity, degradation, impact on cell behavior and mechanical performances. We first considered the influence of the composition alone, and then the influence of both parameters. We demonstrated that the composition affects surface properties, degradation rates and mechanical performance, and as a result, impacts cell attachment, proliferation and osteogenic differentiation. When combined with the porosity for 3D constructs, a synergistic effect of both parameters can be highlighted on the mechanical performances. However, based on this study, no optimal composition or porosity can be identified, and both parameters should be selected regarding the application. In this regard, the results of this study can provide guidance during the design process. As a proof of concept, we finally designed a construct for intervertebral disk replacement that integrates multiple compositions and porosities. Because FDM 3D printing is used, its manufacturing is possible in a single piece, the feasibility being illustrated with a prototype.

In the end, this study enlarges the scope of FDM 3D printing for bone tissue engineering applications, by providing guidance for the design of PCL/β-TCP constructs and proving the feasibility of single piece constructs integrating multiple porosities and composite compositions. It potentially leads the way towards the development of novel designs, for instance implants specific not only to the patient but also to the type of bone.

Supplementary Material

Refer to Web version on PubMed Central for supplementary material.

Acknowledgments

We would like to acknowledge the financial support of the following agencies and donors: NIH R01AR057837 (NIAMS), NIH 1U01AR069395 (NIAMS/NIBIB), Stanford Coulter Translational Seed Grant, Boswell Foundation, and Kent Thiry and Denise O'Leary.

Bibliography

1. Hutmacher DW. Scaffolds in tissue engineering bone and cartilage. Biomaterials. 2000; 25(24):29–43.
2. Lichte P, Pape HC, Pufe T, Kobbe P, Fischer H. Scaffolds for bone healing: Concepts, materials and evidence. Injury. 2011; 42:569–573. [PubMed: 21489531]
3. Stevens B, Yang Y, Mohandas A, Stucker B, Nguyen TK. A review of materials, fabrication methods, and strategies used to enhance bone regeneration in engineered bone tissues. J Biomed Mater Res. 2011; 85B:573–582.
4. Bose S, Vahabzadeh S, Bandyopadhyay A. Bone tissue engineering using 3D printing. Materials Today. 2013; 16(12):496–504.
5. Kawai T, Shanjani Y, Fazeli S, Behn AW, Okuzu Y, Goodman SB, Yang YP. Customized, degradable, functionally graded scaffold for potential treatment of early stage osteonecrosis of the femoral head. Journal of Orthopaedic Research. 2017; 35:23673.
6. Singh S, Ramakrishna S. Biomedical applications of additive manufacturing: present and future. Current Opinion in Biomedical Engineering. 2017; 2:105–115.
7. Elomaa L, Yang YP. Additive manufacturing of vascular grafts and vascularized tissue constructs. Tissue Eng Part B Rev. 2017; 23(5):436–450. [PubMed: 27981886]

8. Hutmacher DW, Schantz T, Zein I, Ng KW, Teoh SH, Tan KC. Mechanical properties and cell cultural response of polycaprolactone scaffolds designed and fabricated via fused deposition modeling. J Biomed Mater Res. 2001; 55:203–216. [PubMed: 11255172]

9. Goyanes A, Buanz ABM, Basit A, Gaisford S. Fused-filament 3D printing (3DP) for fabrication of tablets. International Journal of Pharmaceutics. 2014; 476:88–92. [PubMed: 25275937]

10. Zein I, Hutmacher DW, Tan KC, Teoh SH. Fused deposition modeling of novel scaffold architectures for tissue engineering applications. Biomaterials. 2002; 23:1169–1185. [PubMed: 11791921]

11. Marrella A, Lee TY, Lee DH, Karuthedom S, Syla D, Chawla A, Khademhosseini A, Jang HL. Engineering vascularized and innervated bone biomaterials for improved skeletal tissue regeneration. Materials Today. 2017; 2017

12. Shanjani Y, Kang Y, Zarnescu L, Ellerbee Bowden AK, Koh JT, Ker DFE, Yang Y. Endothelial pattern formation in hybrid constructs of additive manufactured porous rigid scaffolds and cell-laden hydrogels for orthopedic applications. Journal of the Mechanical Behavior of Biomedical Materials. 2017; 65:356–372. [PubMed: 27631173]

13. Woodruff MA, Hutmacher DW. The return of a forgotten polymer—Polycaprolactone in the 21st century. Progress in Polymer Science. 2010; 35:1217–1256.

14. Huang B, Caetano G, Vyas C, Blaker JJ, Diver C, Bártolo P. Polymer-Ceramic Composite Scaffolds: The Effect of Hydroxyapatite and β-tri-Calcium Phosphate. Materials. 2018; 11(1):129.

15. Legeros RZ. Calcium Phosphate-Based Osteoinductive Materials. Chemical Reviews. 2008; 108(11):4742–4753. [PubMed: 19006399]

16. Yeo A, Rai B, Sju E, Cheong JJ, Teoh SH. The degradation profile of novel, bioresorbable PCL–TCP scaffolds: An in vitro and in vivo study. J Biomed Mater Res. 2008; 84A:208–218.

17. Lee H, Kim GH. Three-dimensional plotted PCL/β-TCP scaffolds coated with a collagen layer: preparation, physical properties and in vitro evaluation for bone tissue regeneration. Journal of Materials Chemistry. 2011; 21.17:6305–6312.

18. Lei Y, Rai B, Ho KH, Teoh SH. In vitro degradation of novel bioactive polycaprolactone—20% tricalcium phosphate composite scaffolds for bone engineering. Materials Science and Engineering: C. 2007; 27:293–298.

19. Hollister SJ. Porous scaffold design for tissue engineering. Nature Materials. 2005; 4:518–524. [PubMed: 16003400]

20. Hollister SJ, Maddox RD, Taboas JM. Optimal design and fabrication of scaffolds to mimic tissue properties and satisfy biological constraints. Biomaterials. 2002; 23:4095–4103. [PubMed: 12182311]

21. Shin YM, Park JS, Jeong SI, An SJ, Gwon HJ, Lim YM. Promotion of Human Mesenchymal Stem Cell Differentiation on Bioresorbable Polycaprolactone/Biphasic Calcium Phosphate Composite Scaffolds for Bone Tissue Engineering. Biotechnol Bioproc E. 2014; 19:341–349.

22. Lepoittevin B, Devalckenaere M, Pantoustier N, Alexandre M, Kubies D, Calberg C, Jerome R, Dubois P. Poly(ε-caprolactone)/clay nanocomposites prepared by melt intercalation: mechanical, thermal and rheological properties. Polymer. 2002; 43:4017–4023.

23. Lam CX, Teoh SH, Hutmacher DW. Comparison of the degradation of polycaprolactone and polycaprolactone–(β-tricalcium phosphate) scaffolds in alkaline medium. Polym Int. 2007; 56:718–728.

24. Li SM, Chen XH, Gross RA, McCarthy SP. Hydrolytic degradation of PCL/PEO copolymers in alkaline media. Journal of Materials Science: Materials in Medicine. 2000; 11:227–233. [PubMed: 15348037]

25. Polini A, Pisignano D, Parodi M, Quarto R, Scaglione S. Osteoinduction of Human Mesenchymal Stem Cells by Bioactive Composite Scaffolds without Supplemental Osteogenic Growth Factors. PLoS One. 2011; 6(10)

26. Mirhadi S, Ashwood N, Karagkevrekis B. Factors influencing fracture healing. Trauma. 2013; 15:140–155.

27. Nielsen LE. Mechanical properties of particulate-filled systems. Journal of Composite Materials. 1967; 1:100–119.

28. Gibson LJ. The mechanical behaviour of cancellous bone. Journal of Biomechanics. 1985; 18:317–328. [PubMed: 4008502]

29. Serhan H, Mhatre D, Defossez H, Bono CM. Motion-preserving technologies for degenerative lumbar spine: The past, present, and future horizons. SAS J. 2011; 5(3):75–89. [PubMed: 25802672]

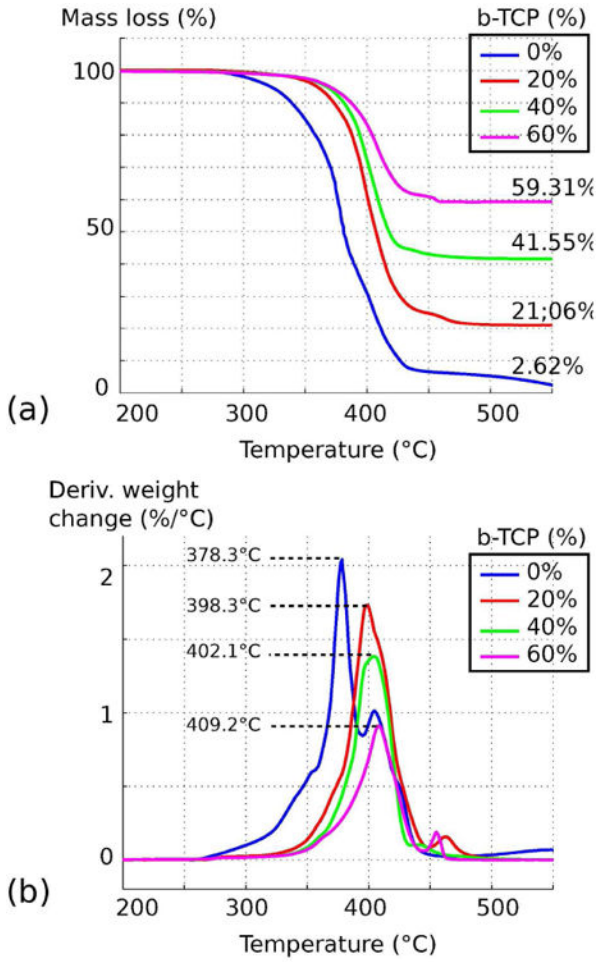

Fig. 1.

Thermogravimetric analysis of PCL/β-TCP composites with a theoretical ceramic composition of 0%, 20%, 40%, 60%. (a) Variation of mass loss according to temperature. (b) Differential thermogravimetric analysis.

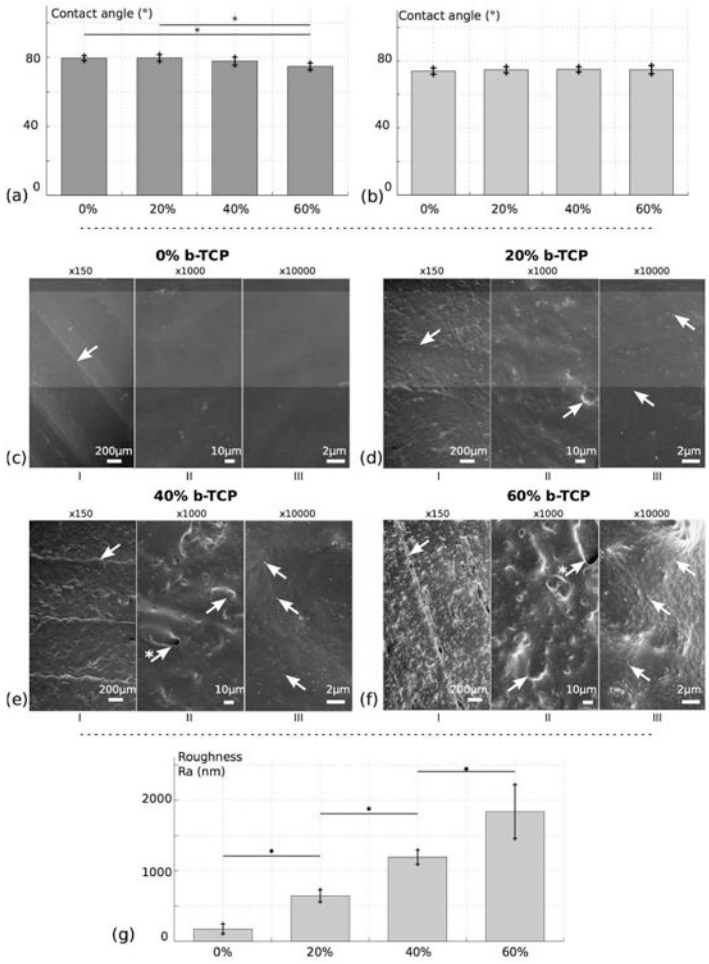

Fig. 2.

Surface analysis of 3D printed PCL/β-TCP scaffolds with different ceramic amount: 0%, 20%, 40%, 60%. (a) Contact angle measurement after post-processing. (b) Contact angle measurement without post-processing. (c) to (f) SEM imaging of the scaffolds for respective composition of 0%, 20%, 40%, 60%. (g) Surface roughness measurement Ra for the different ratios. For SEM, different magnifications are observed: ×150 (I), ×1000 (II) and ×10000 (III). In (I), arrows indicate linear ridges resulting from 3D printing. In (II), arrows highlight ceramic aggregates, sometimes resulting in holes at the surface (arrows marked with *). In (III), arrows are pointing towards β-TCP nanoscopic particles.

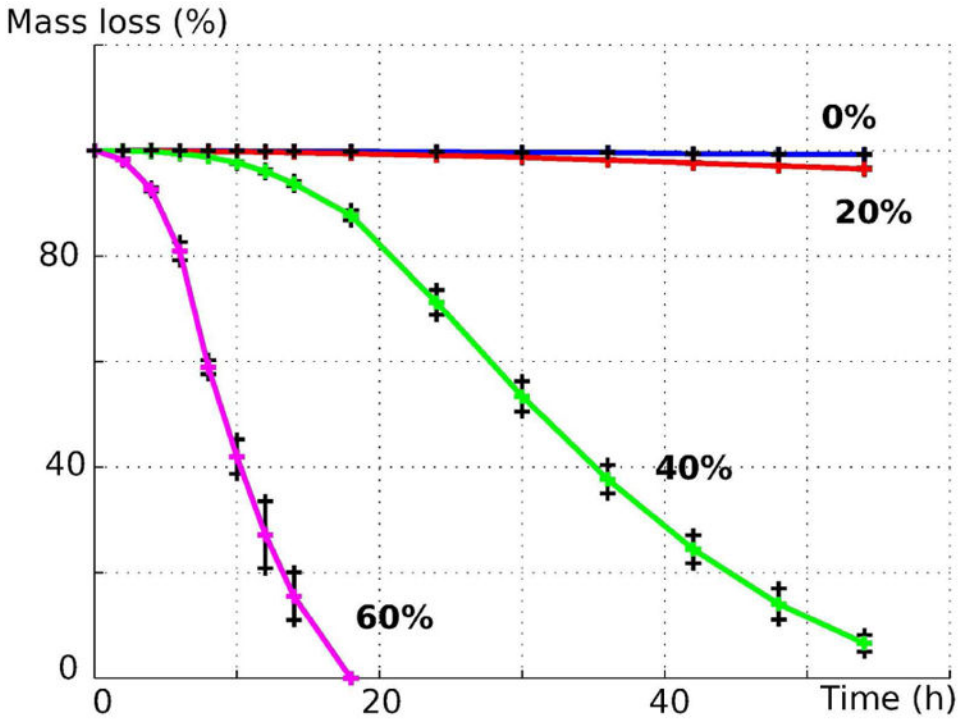

Fig. 3.

Accelerated degradation of PCL/β-TCP material under alkaline conditions for ceramic composition of 0%, 20%, 40% and 60%.

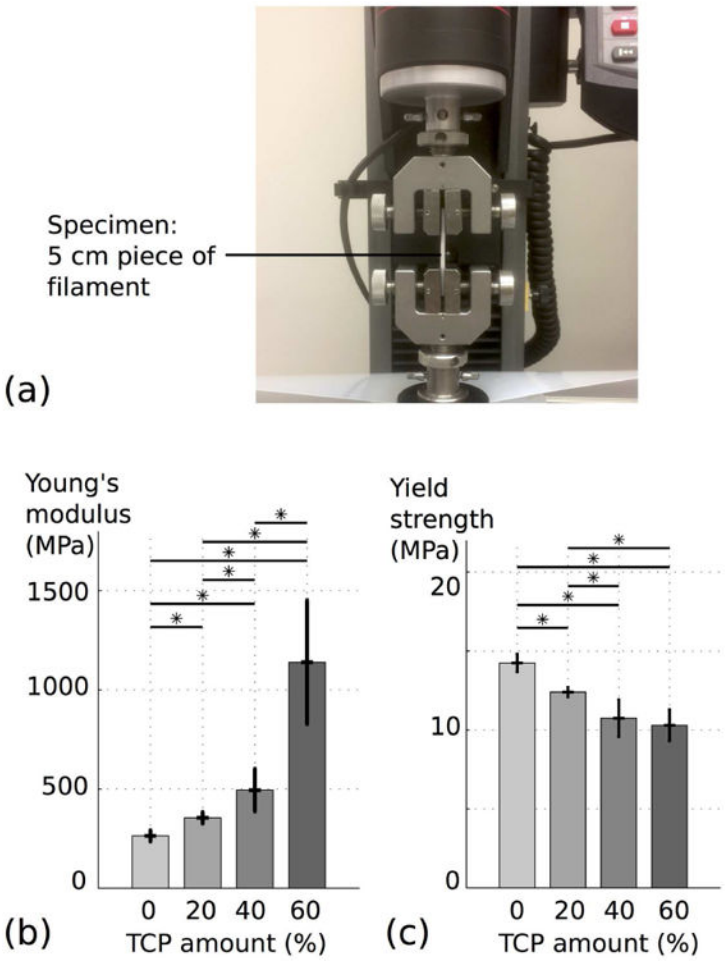

Fig. 4.

Tensile testing of PCL/β-TCP filaments with different ceramic amounts: 0%, 20%, 40%, 60%. (a) Experimental setup. (b) and (c) Evolution of respectively the Young's modulus and the yield strength according to the amount of β-TCP.

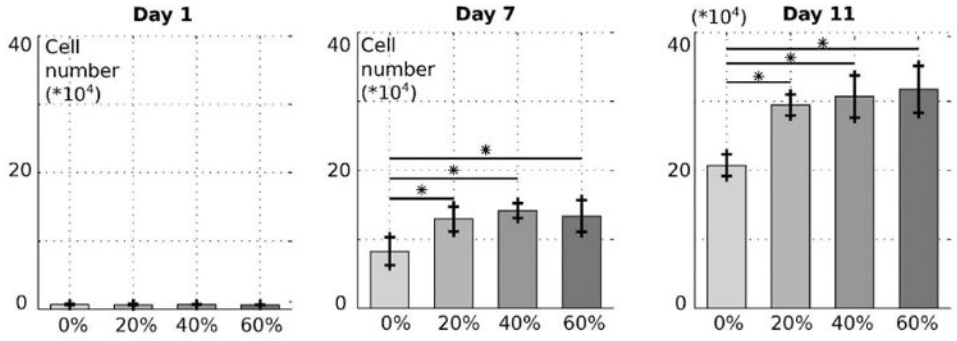

Fig. 5.

Proliferation of C3H10 mouse fibroblasts on 3D printed PCL/β-TCP surfaces with different ceramic amounts: 0%, 20%, 40%, 60%. Cells were counted at Day 1, 7 and 11 for each composition.

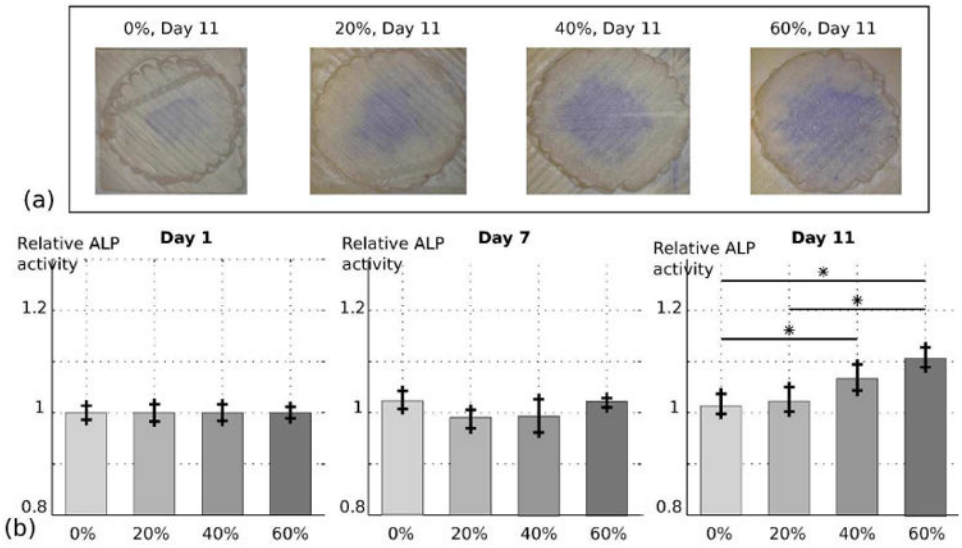

Fig. 6.

Semi-quantitative evaluation of the ALP activity of C3H10 mouse fibroblasts on 3D printed PCL/β-TCP surfaces with different ceramic amounts: 0%, 20%, 40%, 60%. (a) Scaffolds of different compositions after staining at day 11. (b) Image quantification of the ALP activity at day 1, 7 and 11.

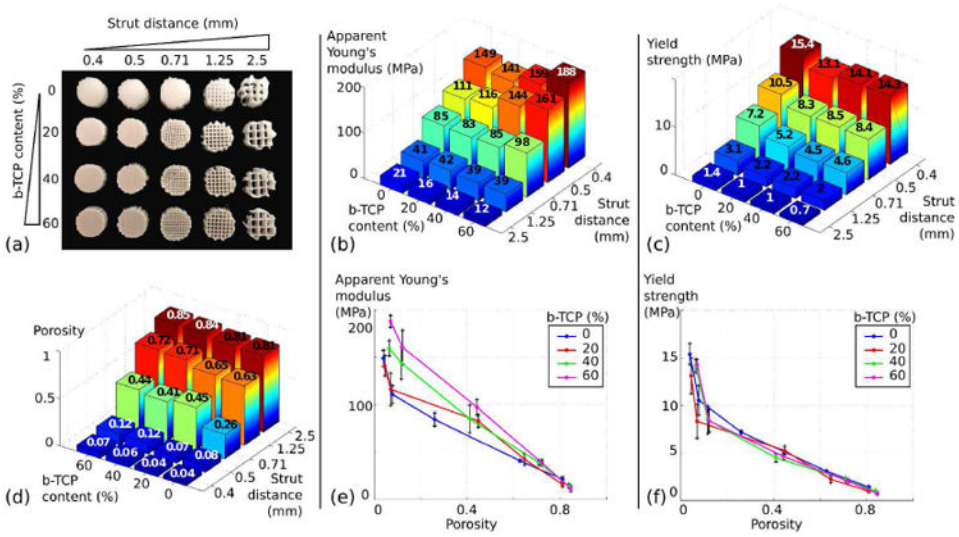

Fig. 7.

Systematic characterization of the influence of porosity and composition of 3D printed constructs on the mechanical performances. (a) Example of scaffolds for each of the 20 groups studied. (b) and (c) Respective evolution of the apparent Young's modulus and the yield strength regarding the composition of the scaffold and the strut distance. (d) Assessment of the porosity of each scaffolds using μ-CT images. (e) and (f) Respective evolution of the apparent Young's modulus and the yield strength according to the porosity for each composition.

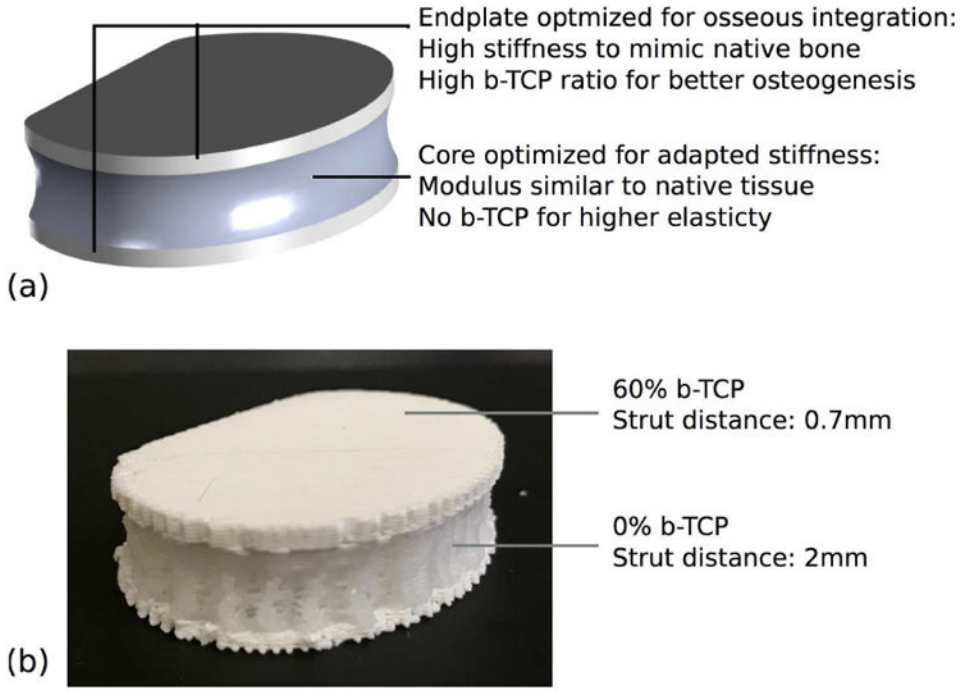

Fig. 8.

Novel design of a 3D printed disc implant. (a) Design explanation and CAD model of the overall volume. (b) Prototype after 3D printing.